

Observation of a neutral charmoniumlike state $Z_c(4025)^0$ in $e^+e^- \rightarrow (D^*\bar{D}^*)^0\pi^0$

M. Ablikim¹, M. N. Achasov^{9,f}, X. C. Ai¹, O. Albayrak⁵, M. Albrecht⁴, D. J. Ambrose⁴⁴, A. Amoroso^{48A,48C}, F. F. An¹, Q. An^{45,a}, J. Z. Bai¹, R. Baldini Ferroli^{20A}, Y. Ban³¹, D. W. Bennett¹⁹, J. V. Bennett⁵, M. Bertani^{20A}, D. Bettoni^{21A}, J. M. Bian⁴³, F. Bianchi^{48A,48C}, E. Boger^{23,d}, I. Boyko²³, R. A. Briere⁵, H. Cai⁵⁰, X. Cai^{1,a}, O. Cakir^{40A,b}, A. Calcaterra^{20A}, G. F. Cao¹, S. A. Cetin^{40B}, J. F. Chang^{1,a}, G. Chelkov^{23,d,e}, G. Chen¹, H. S. Chen¹, H. Y. Chen², J. C. Chen¹, M. L. Chen^{1,a}, S. J. Chen²⁹, X. Chen^{1,a}, X. R. Chen²⁶, Y. B. Chen^{1,a}, H. P. Cheng¹⁷, X. K. Chu³¹, G. Cibinetto^{21A}, H. L. Dai^{1,a}, J. P. Dai³⁴, A. Dbeysy¹⁴, D. Dedovich²³, Z. Y. Deng¹, A. Denig²², I. Denysenko²³, M. Destefanis^{48A,48C}, F. De Mori^{48A,48C}, Y. Ding²⁷, C. Dong³⁰, J. Dong^{1,a}, L. Y. Dong¹, M. Y. Dong^{1,a}, S. X. Du⁵², P. F. Duan¹, E. E. Eren^{40B}, J. Z. Fan³⁹, J. Fang^{1,a}, S. S. Fang¹, X. Fang^{45,a}, Y. Fang¹, L. Fava^{48B,48C}, F. Feldbauer²², G. Felici^{20A}, C. Q. Feng^{45,a}, E. Fioravanti^{21A}, M. Fritsch^{14,22}, C. D. Fu¹, Q. Gao¹, X. Y. Gao², Y. Gao³⁹, Z. Gao^{45,a}, I. Garzia^{21A}, C. Geng^{45,a}, K. Goetzen¹⁰, W. X. Gong^{1,a}, W. Gradl²², M. Greco^{48A,48C}, M. H. Gu^{1,a}, Y. T. Gu¹², Y. H. Guan¹, A. Q. Guo¹, L. B. Guo²⁸, Y. Guo¹, Y. P. Guo²², Z. Haddadi²⁵, A. Hafner²², S. Han⁵⁰, Y. L. Han¹, X. Q. Hao¹⁵, F. A. Harris⁴², K. L. He¹, Z. Y. He³⁰, T. Held⁴, Y. K. Heng^{1,a}, Z. L. Hou¹, C. Hu²⁸, H. M. Hu¹, J. F. Hu^{48A,48C}, T. Hu^{1,a}, Y. Hu¹, G. M. Huang⁶, G. S. Huang^{45,a}, H. P. Huang⁵⁰, J. S. Huang¹⁵, X. T. Huang³³, Y. Huang²⁹, T. Hussain⁴⁷, Q. Ji¹, Q. P. Ji³⁰, X. B. Ji¹, X. L. Ji^{1,a}, L. L. Jiang¹, L. W. Jiang⁵⁰, X. S. Jiang^{1,a}, X. Y. Jiang³⁰, J. B. Jiao³³, Z. Jiao¹⁷, D. P. Jin^{1,a}, S. Jin¹, T. Johansson⁴⁹, A. Julin⁴³, N. Kalantar-Nayestanaki²⁵, X. L. Kang¹, X. S. Kang³⁰, M. Kavatsyuk²⁵, B. C. Ke⁵, P. Kiese²², R. Kliemt¹⁴, B. Kloss²², O. B. Kolcu^{40B,i}, B. Kopf⁴, M. Kornicer⁴², W. Kühn²⁴, A. Kupsc⁴⁹, J. S. Lange²⁴, M. Lara¹⁹, P. Larin¹⁴, C. Leng^{48C}, C. Li⁴⁹, C. H. Li¹, Cheng Li^{45,a}, D. M. Li⁵², F. Li^{1,a}, G. Li¹, H. B. Li¹, J. C. Li¹, Jin Li³², K. Li¹³, K. Li³³, Lei Li³, P. R. Li⁴¹, T. Li³³, W. D. Li¹, W. G. Li¹, X. L. Li³³, X. M. Li¹², X. N. Li^{1,a}, X. Q. Li³⁰, Z. B. Li³⁸, H. Liang^{45,a}, Y. F. Liang³⁶, Y. T. Liang²⁴, G. R. Liao¹¹, D. X. Lin¹⁴, B. J. Liu¹, C. X. Liu¹, F. H. Liu³⁵, Fang Liu¹, Feng Liu⁶, H. B. Liu¹², H. H. Liu¹⁶, H. H. Liu¹, H. M. Liu¹, J. Liu¹, J. B. Liu^{45,a}, J. P. Liu⁵⁰, J. Y. Liu¹, K. Li³⁹, K. Y. Liu²⁷, L. D. Liu^{31*}, P. L. Liu^{1,a}, Q. Liu⁴¹, S. B. Liu^{45,a}, X. Liu²⁶, X. X. Liu⁴¹, Y. B. Liu³⁰, Z. A. Liu^{1,a}, Zhiqiang Liu¹, Zhiqing Liu²², H. Loehner²⁵, X. C. Lou^{1,a,h}, H. J. Lu¹⁷, J. G. Lu^{1,a}, R. Q. Lu¹⁸, Y. Lu¹, Y. P. Lu^{1,a}, C. L. Luo²⁸, M. X. Luo⁵¹, T. Luo⁴², X. L. Luo^{1,a}, M. Lv¹, X. R. Lyu⁴¹, F. C. Ma²⁷, H. L. Ma¹, L. L. Ma³³, Q. M. Ma¹, T. Ma¹, X. N. Ma³⁰, X. Y. Ma^{1,a}, F. E. Maas¹⁴, M. Maggiora^{48A,48C}, Y. J. Mao³¹, Z. P. Mao¹, S. Marcello^{48A,48C}, J. G. Messchendorp²⁵, J. Min^{1,a}, T. J. Min¹, R. E. Mitchell¹⁹, X. H. Mo^{1,a}, Y. J. Mo⁶, C. Morales Morales¹⁴, K. Moriya¹⁹, N. Yu. Muchnoi^{9,f}, H. Muramatsu⁴³, Y. Nefedov²³, F. Nerling¹⁴, I. B. Nikolaev^{9,f}, Z. Ning^{1,a}, S. Nisar⁸, S. L. Niu^{1,a}, X. Y. Niu¹, S. L. Olsen³², Q. Ouyang^{1,a}, S. Pacetti^{20B}, P. Patteri^{20A}, M. Pelizaeus⁴, H. P. Peng^{45,a}, K. Peters¹⁰, J. Pettersson⁴⁹, J. L. Ping²⁸, R. G. Ping¹, R. Poling⁴³, V. Prasad¹, Y. N. Pu¹⁸, M. Qi²⁹, S. Qian^{1,a}, C. F. Qiao⁴¹, L. Q. Qin³³, N. Qin⁵⁰, X. S. Qin¹, Y. Qin³¹, Z. H. Qin^{1,a}, J. F. Qiu¹, K. H. Rashid⁴⁷, C. F. Redmer²², H. L. Ren¹⁸, M. Ripka²², G. Rong¹, Ch. Rosner¹⁴, X. D. Ruan¹², V. Santoro^{21A}, A. Sarantsev^{23,g}, M. Savriko^{21B}, K. Schoenning⁴⁹, S. Schumann²², W. Shan³¹, M. Shao^{45,a}, C. P. Shen², P. X. Shen³⁰, X. Y. Shen¹, H. Y. Sheng¹, W. M. Song¹, X. Y. Song¹, S. Sosio^{48A,48C}, S. Spataro^{48A,48C}, G. X. Sun¹, J. F. Sun¹⁵, S. S. Sun¹, Y. J. Sun^{45,a}, Y. Z. Sun¹, Z. J. Sun^{1,a}, Z. T. Sun¹⁹, C. J. Tang³⁶, X. Tang¹, I. Tapan^{40C}, E. H. Thorndike⁴⁴, M. Tiemens²⁵, M. Ullrich²⁴, I. Uman^{40B}, G. S. Varner⁴², B. Wang³⁰, B. L. Wang⁴¹, D. Wang³¹, D. Y. Wang³¹, K. Wang^{1,a}, L. L. Wang¹, L. S. Wang¹, M. Wang³³, P. Wang¹, P. L. Wang¹, S. G. Wang³¹, W. Wang^{1,a}, X. F. Wang³⁹, Y. D. Wang¹⁴, Y. F. Wang^{1,a}, Y. Q. Wang²², Z. Wang^{1,a}, Z. G. Wang^{1,a}, Z. H. Wang^{45,a}, Z. Y. Wang¹, T. Weber²², D. H. Wei¹¹, J. B. Wei³¹, P. Weidenkaff²², S. P. Wen¹, U. Wiedner⁴, M. Wolke⁴⁹, L. H. Wu¹, Z. Wu^{1,a}, L. G. Xia³⁹, Y. Xia¹⁸, D. Xiao¹, Z. J. Xiao²⁸, Y. G. Xie^{1,a}, Q. L. Xiu^{1,a}, G. F. Xu¹, L. Xu¹, Q. J. Xu¹³, Q. N. Xu⁴¹, X. P. Xu³⁷, L. Yan^{45,a}, W. B. Yan^{45,a}, W. C. Yan^{45,a}, Y. H. Yan¹⁸, H. J. Yang³⁴, H. X. Yang¹, L. Yang⁵⁰, Y. Yang⁶, Y. X. Yang¹¹, H. Ye¹, M. Ye^{1,a}, M. H. Ye⁷, J. H. Yin¹, B. X. Yu^{1,a}, C. X. Yu³⁰, H. W. Yu³¹, J. S. Yu²⁶, C. Z. Yuan¹, W. L. Yuan²⁹, Y. Yuan¹, A. Yuncu^{40B,c}, A. A. Zafar⁴⁷, A. Zallo^{20A}, Y. Zeng¹⁸, B. X. Zhang¹, B. Y. Zhang^{1,a}, C. Zhang²⁹, C. C. Zhang¹, D. H. Zhang¹, H. H. Zhang³⁸, H. Y. Zhang^{1,a}, J. J. Zhang¹, J. L. Zhang¹, J. Q. Zhang¹, J. W. Zhang^{1,a}, J. Y. Zhang¹, J. Z. Zhang¹, K. Zhang¹, L. Zhang¹, S. H. Zhang¹, X. Y. Zhang³³, Y. Zhang¹, Y. N. Zhang⁴¹, Y. H. Zhang^{1,a}, Y. T. Zhang^{45,a}, Yu Zhang⁴¹, Z. H. Zhang⁶, Z. P. Zhang⁴⁵, Z. Y. Zhang⁵⁰, G. Zhao¹, J. W. Zhao^{1,a}, J. Y. Zhao¹, J. Z. Zhao^{1,a}, Lei Zhao^{45,a}, Ling Zhao¹, M. G. Zhao³⁰, Q. Zhao¹, Q. W. Zhao¹, S. J. Zhao⁵², T. C. Zhao¹, Y. B. Zhao^{1,a}, Z. G. Zhao^{45,a}, A. Zhemchugov^{23,d}, B. Zheng⁴⁶, J. P. Zheng^{1,a}, W. J. Zheng³³, Y. H. Zheng⁴¹, B. Zhong²⁸, L. Zhou^{1,a}, Li Zhou³⁰, X. Zhou⁵⁰, X. K. Zhou^{45,a}, X. R. Zhou^{45,a}, X. Y. Zhou¹, K. Zhu¹, K. J. Zhu^{1,a}, S. Zhu¹, X. L. Zhu³⁹, Y. C. Zhu^{45,a}, Y. S. Zhu¹, Z. A. Zhu¹, J. Zhuang^{1,a}, L. Zotti^{48A,48C}, B. S. Zou¹, J. H. Zou¹

(BESIII Collaboration)

¹ Institute of High Energy Physics, Beijing 100049, People's Republic of China

² Beihang University, Beijing 100191, People's Republic of China

³ Beijing Institute of Petrochemical Technology, Beijing 102617, People's Republic of China

⁴ Bochum Ruhr-University, D-44780 Bochum, Germany

⁵ Carnegie Mellon University, Pittsburgh, Pennsylvania 15213, USA

⁶ Central China Normal University, Wuhan 430079, People's Republic of China

⁷ China Center of Advanced Science and Technology, Beijing 100190, People's Republic of China

⁸ COMSATS Institute of Information Technology, Lahore, Defence Road, Off Raiwind Road, 54000 Lahore, Pakistan

⁹ G.I. Budker Institute of Nuclear Physics SB RAS (BINP), Novosibirsk 630090, Russia

¹⁰ GSI Helmholtzcentre for Heavy Ion Research GmbH, D-64291 Darmstadt, Germany

¹¹ Guangxi Normal University, Guilin 541004, People's Republic of China

¹² GuangXi University, Nanning 530004, People's Republic of China

- ¹³ Hangzhou Normal University, Hangzhou 310036, People's Republic of China
- ¹⁴ Helmholtz Institute Mainz, Johann-Joachim-Becher-Weg 45, D-55099 Mainz, Germany
- ¹⁵ Henan Normal University, Xinxiang 453007, People's Republic of China
- ¹⁶ Henan University of Science and Technology, Luoyang 471003, People's Republic of China
- ¹⁷ Huangshan College, Huangshan 245000, People's Republic of China
- ¹⁸ Hunan University, Changsha 410082, People's Republic of China
- ¹⁹ Indiana University, Bloomington, Indiana 47405, USA
- ²⁰ (A)INFN Laboratori Nazionali di Frascati, I-00044, Frascati, Italy; (B)INFN and University of Perugia, I-06100, Perugia, Italy
- ²¹ (A)INFN Sezione di Ferrara, I-44122, Ferrara, Italy; (B)University of Ferrara, I-44122, Ferrara, Italy
- ²² Johannes Gutenberg University of Mainz, Johann-Joachim-Becher-Weg 45, D-55099 Mainz, Germany
- ²³ Joint Institute for Nuclear Research, 141980 Dubna, Moscow region, Russia
- ²⁴ Justus Liebig University Giessen, II. Physikalisches Institut, Heinrich-Buff-Ring 16, D-35392 Giessen, Germany
- ²⁵ KVI-CART, University of Groningen, NL-9747 AA Groningen, The Netherlands
- ²⁶ Lanzhou University, Lanzhou 730000, People's Republic of China
- ²⁷ Liaoning University, Shenyang 110036, People's Republic of China
- ²⁸ Nanjing Normal University, Nanjing 210023, People's Republic of China
- ²⁹ Nanjing University, Nanjing 210093, People's Republic of China
- ³⁰ Nankai University, Tianjin 300071, People's Republic of China
- ³¹ Peking University, Beijing 100871, People's Republic of China
- ³² Seoul National University, Seoul, 151-747 Korea
- ³³ Shandong University, Jinan 250100, People's Republic of China
- ³⁴ Shanghai Jiao Tong University, Shanghai 200240, People's Republic of China
- ³⁵ Shanxi University, Taiyuan 030006, People's Republic of China
- ³⁶ Sichuan University, Chengdu 610064, People's Republic of China
- ³⁷ Soochow University, Suzhou 215006, People's Republic of China
- ³⁸ Sun Yat-Sen University, Guangzhou 510275, People's Republic of China
- ³⁹ Tsinghua University, Beijing 100084, People's Republic of China
- ⁴⁰ (A)Istanbul Aydin University, 34295 Sefakoy, Istanbul, Turkey; (B)Dogus University, 34722 Istanbul, Turkey; (C)Uludag University, 16059 Bursa, Turkey
- ⁴¹ University of Chinese Academy of Sciences, Beijing 100049, People's Republic of China
- ⁴² University of Hawaii, Honolulu, Hawaii 96822, USA
- ⁴³ University of Minnesota, Minneapolis, Minnesota 55455, USA
- ⁴⁴ University of Rochester, Rochester, New York 14627, USA
- ⁴⁵ University of Science and Technology of China, Hefei 230026, People's Republic of China
- ⁴⁶ University of South China, Hengyang 421001, People's Republic of China
- ⁴⁷ University of the Punjab, Lahore-54590, Pakistan
- ⁴⁸ (A)University of Turin, I-10125, Turin, Italy; (B)University of Eastern Piedmont, I-15121, Alessandria, Italy; (C)INFN, I-10125, Turin, Italy
- ⁴⁹ Uppsala University, Box 516, SE-75120 Uppsala, Sweden
- ⁵⁰ Wuhan University, Wuhan 430072, People's Republic of China
- ⁵¹ Zhejiang University, Hangzhou 310027, People's Republic of China
- ⁵² Zhengzhou University, Zhengzhou 450001, People's Republic of China
- ^a Also at State Key Laboratory of Particle Detection and Electronics, Beijing 100049, Hefei 230026, People's Republic of China
- ^b Also at Ankara University, 06100 Tandogan, Ankara, Turkey
- ^c Also at Bogazici University, 34342 Istanbul, Turkey
- ^d Also at the Moscow Institute of Physics and Technology, Moscow 141700, Russia
- ^e Also at the Functional Electronics Laboratory, Tomsk State University, Tomsk, 634050, Russia
- ^f Also at the Novosibirsk State University, Novosibirsk, 630090, Russia
- ^g Also at the NRC "Kurchatov Institute, PNPI, 188300, Gatchina, Russia
- ^h Also at University of Texas at Dallas, Richardson, Texas 75083, USA
- ⁱ Currently at Istanbul Arel University, 34295 Istanbul, Turkey

We report a study of the process $e^+e^- \rightarrow (D^*\bar{D}^*)^0\pi^0$ using e^+e^- collision data samples with integrated luminosities of 1092 pb^{-1} at $\sqrt{s} = 4.23\text{ GeV}$ and 826 pb^{-1} at $\sqrt{s} = 4.26\text{ GeV}$ collected with the BESIII detector at the BEPCII storage ring. We observe a new neutral structure near the $(D^*\bar{D}^*)^0$ mass threshold in the π^0 recoil mass spectrum, which we denote as $Z_c(4025)^0$. Assuming a

Breit-Wigner line shape, its pole mass and pole width are determined to be $(4025.5^{+2.0}_{-4.7} \pm 3.1)$ MeV/ c^2 and $(23.0 \pm 6.0 \pm 1.0)$ MeV, respectively. The Born cross sections of $e^+e^- \rightarrow Z_c(4025)^0\pi^0 \rightarrow (D^*\bar{D}^*)^0\pi^0$ are measured to be $(61.6 \pm 8.2 \pm 9.0)$ pb at $\sqrt{s} = 4.23$ GeV and $(43.4 \pm 8.0 \pm 5.4)$ pb at $\sqrt{s} = 4.26$ GeV. The first uncertainties are statistical and the second are systematic.

PACS numbers: 14.40.Rt, 13.25.Gv, 13.66.Bc

Recent discoveries of new charmoniumlike states that do not fit naturally with the predictions of the quark model have generated great experimental and theoretical interests [1]. Among these so-called “ XYZ ” particles are charged states with decay modes that clearly demonstrate a structure consisting of at least four quarks, including a $c\bar{c}$ pair. The first charged charmoniumlike state $Z(4430)^+$ was discovered by Belle [2]. LHCb confirmed the existence of this state. Belle determined its spin-parity to be 1^+ [3], which is supported by a new result from LHCb[4]. Recently, the BESIII collaboration observed four charged Z_c states, $Z_c(3885)^\pm$ [5], $Z_c(3900)^\pm$ [6], $Z_c(4020)^\pm$ [7], and $Z_c(4025)^\pm$ [8], produced in $e^+e^- \rightarrow \pi^\mp Z_c^\pm$. The observed decay channels are $Z_c(3900)^\pm \rightarrow \pi^\pm J/\psi$, $Z_c(3885)^\pm \rightarrow (D\bar{D}^*)^\pm$, $Z_c(4020)^\pm \rightarrow \pi^\pm h_c$, and $Z_c(4025)^\pm \rightarrow (D^*\bar{D}^*)^\pm$. These states are close to the $D\bar{D}^*$ or $D^*\bar{D}^*$ threshold. The $Z_c(3900)^\pm$ was also observed by Belle [9] and with CLEO-c data [10].

So far, the nature of these new states is still elusive. Interpretations in terms of tetra-quarks, molecules, hadro-charmonium, and cusp effects have been proposed [11–19]. Searching for their neutral partners in experiment is of great importance to understand their properties, especially to identify their isospin properties. Previously, based on CLEO-c data, evidence of a neutral state $Z_c(3900)^0$ decaying to $\pi^0 J/\psi$ [20] was reported. Recently, two neutral states, $Z_c(3900)^0$ and $Z_c(4020)^0$, were discovered in their decays $Z_c(3900)^0 \rightarrow \pi^0 J/\psi$ and $Z_c(4020)^0 \rightarrow \pi^0 h_c$ by BESIII [21, 22]. These can be interpreted as the isospin partners of the $Z_c(3900)^\pm$ and $Z_c(4020)^\pm$. Analogously, it is natural to search for the neutral partner of the $Z_c(4025)^\pm$ [8] in its decay to $(D^*\bar{D}^*)^0$.

In this Letter, we report a search for the neutral partner of the $Z_c(4025)^\pm$ through the reactions $e^+e^- \rightarrow D^{*0}\bar{D}^{*0}(D^{*+}D^{*-})\pi^0$, as the charged $Z_c(4025)^\pm$ [8] couples to $(D^*\bar{D}^*)^\pm$ and has a mass close to the $(D^*\bar{D}^*)^\pm$ mass threshold. We denote the investigated final state products as $(D^*\bar{D}^*)^0\pi^0$, where D^* refers to D^{*0} or D^{*+} , and \bar{D}^* stands for their antiparticles. A partial reconstruction method is applied to identify the $(D^*\bar{D}^*)^0\pi^0$ final states. This method requires detection of a D and a \bar{D} originating from D^* and \bar{D}^* decays of $D^* \rightarrow D\pi$ and $D\gamma$, and the π^0 from the primary production (denoted as the *bachelor* π^0). The data sample analyzed corresponds to e^+e^- collisions with integrated luminosities of 1092 pb^{-1} at $\sqrt{s} = 4.23$ GeV and 826 pb^{-1} at $\sqrt{s} = 4.26$ GeV [23] collected with the BESIII detector [24] at the BEPCII storage ring [25].

BESIII is a cylindrically symmetric detector, which

from inner to outer parts consists of the following components: a Helium-gas based multilayer drift chamber (MDC), a time-of-flight counter (TOF), a CsI(Tl) crystal electromagnetic calorimeter (EMC), a 1-Tesla superconducting solenoid magnet and a 9-layer RPC-based muon chamber system. The momentum resolution for charged tracks in the MDC is 0.5% at a momentum of 1 GeV/ c . The energy resolution for photons in EMC with energy of 1 GeV is 2.5% for the center region (barrel) and 5% for the rest of the detector (endcaps). For charged particle identification (PID), probabilities $\mathcal{L}(h)$ for particle hypotheses $h = \pi$ or K are evaluated based on the normalized energy loss dE/dx in the MDC and the time of flight in the TOF. More details on the BESIII spectrometer can be found in Ref. [24].

To optimize data-selection criteria, understand backgrounds and estimate the detection efficiency, we simulate the e^+e^- annihilation processes with the KKMC algorithm [26], which takes into account continuum processes, initial state radiation (ISR) return to ψ and Y states, and inclusive $D_{(s)}$ production. The known decay rates are taken from the Particle Data Group (PDG) [27] and decays are modeled with EVTGEN [28]. The remaining decays are simulated with the LUNDCHARM package [29]. The non-resonant, three-body phase space (PHSP) processes $e^+e^- \rightarrow D^*\bar{D}^*\pi^0$ are simulated according to uniform distributions in momentum phase space. We assume that $Z_c(4025)^0$ has spin-parity of 1^+ by considering the measurements of other Z resonances [3, 4] and the signal process $e^+e^- \rightarrow Z_c(4025)^0\pi^0$ followed by $Z_c(4025)^0 \rightarrow (D^*\bar{D}^*)^0$ proceeds in S waves. The D^* is required to decay inclusively according to its decay branching ratios from PDG [27]. The D^+ is required to decay into $K^-\pi^+\pi^+$ while D^0 is required to decay into $K^-\pi^+$, $K^-\pi^+\pi^0$ and $K^-\pi^+\pi^+\pi^-$. These decay modes are the ones used to reconstruct D mesons [30]. All simulated MC events are fed into a GEANT4-based [31] software package, taking into account detector geometry and response.

The charged tracks of K^- and π^\pm are reconstructed in the MDC. For each charged track, the polar angle θ defined with respect to the e^+ beam is required to satisfy $|\cos\theta| < 0.93$. The closest approach to the e^+e^- interaction point is required to be within ± 10 cm along the beam direction and within 1 cm in the plane perpendicular to the beam direction. A track is identified to be a $K(\pi)$ when the PID probabilities satisfy $\mathcal{L}(K) > \mathcal{L}(\pi)$ ($\mathcal{L}(K) < \mathcal{L}(\pi)$), according to the information from dE/dx and TOF.

The π^0 candidates are reconstructed by combining pairs of photons reconstructed in the EMC that are not

associated with charged tracks. For each photon, the energy deposition in the EMC barrel region is required to be greater than 25 MeV, while in the end-cap region, it must be greater than 50 MeV, due to the different detector resolution and probabilities of reconstructing a fake photon. To suppress electronics noise and energy deposits unrelated to the event, the EMC cluster time is restricted to be within a 700 ns window near the event start time. The invariant mass of any pair of photons $M(\gamma\gamma)$ is required to be within $(0.120, 0.145)$ GeV/ c^2 and constrained to the nominal π^0 mass. The kinematics of the two photons are updated according to the constraint fit.

We consider all possible combinations of selected charged tracks and π^0 to form D candidates. The charged tracks from a D decay candidate are required to originate from a common vertex. The χ^2_{VF} of the vertex fit is required to satisfy $\chi^2_{\text{VF}} < 100$. We constrain the reconstructed masses of the final state particles to the corresponding D nominal masses and require $\chi^2_{\text{KF}}(D)$ for the kinematic fit to be less than 15 for the final states of D decays including charged tracks only, and less than 20 for the final state including π^0 . We select signal event candidates which consist of at least one pair of $D\bar{D}$ candidates that do not share particles in the final state. If there is more than one pair of $D\bar{D}$ candidates in an event, only the one with the minimum $\chi^2_{\text{KF}}(D) + \chi^2_{\text{KF}}(\bar{D})$ is kept for further analysis.

We reconstruct the bachelor π^0 from the remaining photon showers that are not assigned to the $D\bar{D}$ pair. To further reject backgrounds, each photon candidate originating from the bachelor π^0 is required not to form a π^0 candidate with any other photon in the event. A mass constraint of the two photons to the π^0 nominal mass is implemented and the corresponding fit quality is required to satisfy $\chi^2_{\text{KF}}(\pi^0) < 20$. To reject background for the bachelor π^0 from $D^* \rightarrow D\pi^0$ decays, we require the $D\pi^0$ invariant mass to be greater than 2.02 GeV/ c^2 .

To identify the decay products of the signal process $e^+e^- \rightarrow D^*\bar{D}^*\pi^0$, we plot the recoil mass spectra of $D\pi^0$ ($RM(D\pi^0)$), as shown in Fig. 1. The peaks around 2 GeV/ c^2 correspond to the process $e^+e^- \rightarrow D\bar{D}^*\pi^0$ with a missing \bar{D}^* . Besides these peaks, we see clear bumps around 2.15 GeV/ c^2 in data. These bumps are consistent with the MC simulations of the $D^*\bar{D}^*\pi^0$ final state. The peak position roughly corresponds to the sum of the mass of D^* and the mass of a π , since the π originating from D^* is soft and is not used in the computation of the recoil mass. The backgrounds beneath the bumps are mostly from ISR production of $D^*\bar{D}^*$ process. Other processes, such as $e^+e^- \rightarrow D^*\bar{D}^{*0} \rightarrow D^*\bar{D}^*\pi^0$, are expected to be absent according to simulation studies. This is understandable because the process $D_0^*(2400) \rightarrow D^*\pi^0$ is forbidden due to the conservation of spin-parity. $D_1^*(2420)^0$ ($D_2^*(2460)^0$) is narrow, and the sum of the mass of $D_1^*(2420)^0$ ($D_2^*(2460)^0$) and D^* is much larger than 4.26 GeV. To extract the signals, we keep events within the two-dimensional oval regions in the distribu-

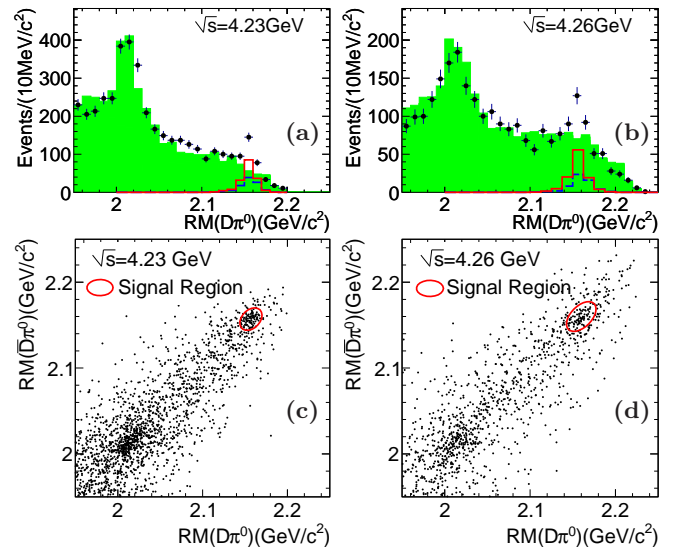


FIG. 1. Distributions of $RM(D\pi^0)$ at $\sqrt{s} = 4.23$ GeV (a) and $\sqrt{s} = 4.26$ GeV (b). Points with error bars are data and the shaded histograms represent the inclusive backgrounds in MC simulations. The solid line and the dashed line are the $Z_c(4025)^0$ signal shape and the PHSP shape with arbitrary normalization, respectively. The third row gives the scatter plot of $RM(D\pi^0)$ versus $RM(\bar{D}\pi^0)$ at $\sqrt{s} = 4.23$ GeV (c) and $\sqrt{s} = 4.26$ GeV (d), where the solid ovals indicate the signal regions.

tions of $RM(D\pi^0)$ and $RM(\bar{D}\pi^0)$ shown in Fig. 1(c,d). We choose the specific dimensions due to different resolutions at different momentum phase spaces at two energy points. They are determined according to MC simulation.

The selected events are used to produce the recoil mass distribution of the bachelor π^0 ($RM(\pi^0)$), shown in Fig. 2. We observe enhancements in the $RM(\pi^0)$ distribution over the inclusive backgrounds for both data samples, which can not be explained by three-body non-resonant processes. We assume the presence of an S -wave Breit-Wigner resonance structure (denoted as $Z_c(4025)^0$) with a mass-dependent width, using the form given in Ref. [32]:

$$\left| \frac{1}{M^2 - m^2 - i \cdot m(\Gamma_1(M) + \Gamma_2(M))/c^2} \right|^2 \cdot p_k \cdot q_k,$$

$$\text{and } \Gamma_k(M) = f_k \cdot \Gamma \cdot \frac{p_k}{p_k^*} \cdot \frac{m}{M} \quad (k = 1, 2).$$

Here, $k = 1$ and 2 denote the neutral channel $Z_c(4025)^0 \rightarrow D^{*0}\bar{D}^{*0}$ and the charged channel $Z_c(4025)^0 \rightarrow D^{*+}D^{*-}$, respectively. f_k is the ratio of the partial decay width for channel k . M is the reconstructed mass, m is the resonance mass and Γ is the resonance width. $p_k(q_k)$ is the $D^*(\pi^0)$ momentum in the rest frame of the $D^*\bar{D}^*$ system (the initial e^+e^- system) and p_k^* is the momentum of D^* in the $Z_c(4025)^0$ rest frame

at $M = m$. We assume that $Z_c(4025)^0$ decay rates to the neutral channel and the charged channel are equal, *i.e.*, $f_k = 0.5$, based on isospin symmetry.

We perform a simultaneous unbinned maximum likelihood fit to the spectra of $RM(\pi^0)$ at $\sqrt{s} = 4.23$ and 4.26 GeV. The signal shapes are taken as convolutions of the efficiency-weighted Breit-Wigner functions with resolution functions obtained from MC simulations. The detector resolutions are 4 MeV at $\sqrt{s} = 4.23$ GeV and 4.5 MeV at $\sqrt{s} = 4.26$ GeV. Backgrounds are modeled with kernel-estimated non-parametric shapes [33] based on the inclusive MC, and their magnitudes are fixed according to the simulations, since the inclusive MC samples well describe the background. The shape of the PHSP process is adopted from MC simulations. We combine the data at $\sqrt{s} = 4.23$ GeV and $\sqrt{s} = 4.26$ GeV together, as shown in Fig. 2. The fit determines m and Γ to be $(4031.7 \pm 2.1) \text{ MeV}/c^2$ and $(25.9 \pm 8.8) \text{ MeV}$, respectively. The corresponding pole position $m_{\text{pole}}(Z_c(4025)^0) - i\frac{\Gamma_{\text{pole}}(Z_c(4025)^0)}{2}$ is calculated to be

$$m_{\text{pole}}(Z_c(4025)^0) = (4025.5_{-4.7}^{+2.0}) \text{ MeV}/c^2,$$

$$\Gamma_{\text{pole}}(Z_c(4025)^0) = (23.0 \pm 6.0) \text{ MeV}.$$

The significance with systematic errors is estimated by comparing the likelihoods of the fits with and without the $Z_c(4025)^0$ signal component included. The likelihood difference is $2\Delta \ln L = 45.3$ and the difference of the number of free parameters is 4. When the systematic uncertainties are taken into account with the assumption of Gaussian distribution, the significance is estimated to be 5.9σ .

The Born cross section $\sigma(e^+e^- \rightarrow Z_c(4025)^0\pi^0 \rightarrow (D^{*0}\bar{D}^{*0} + D^{*+}D^{*-})\pi^0)$ is calculated from the equation

$$\sigma = \frac{n_{\text{sig}}}{\mathcal{L}(f_1\mathcal{B}_1\varepsilon_1 + f_2\mathcal{B}_2\varepsilon_2)(1 + \delta)(1 + \delta_{\text{vac}})},$$

where \mathcal{L} is the integrated luminosity, ε_1 (ε_2) is the detection efficiency of the neutral (charged) channel, f_1 (f_2) is the ratio of the cross section of the neutral (charged) channel to the sum of the both channels, \mathcal{B}_1 (\mathcal{B}_2) is the product branching fraction of the neutral (charged) D^* decays to the final states we detected. $(1 + \delta)$ is the radiative correction factor and $(1 + \delta_{\text{vac}})$ is the vacuum polarization factor. From the simultaneous fit, we obtain 69.5 ± 9.2 signal events at $\sqrt{s} = 4.23$ GeV and 46.1 ± 8.5 signal events at $\sqrt{s} = 4.26$ GeV. $(1 + \delta)$ is calculated to be 0.744 at $\sqrt{s} = 4.23$ GeV and 0.793 at $\sqrt{s} = 4.26$ GeV to the second order in QED [34], where the input line shape of the cross section is assumed to be the same as for $e^+e^- \rightarrow (D^*\bar{D}^*)^+\pi^-$, as extracted directly from BESIII data. $(1 + \delta_{\text{vac}})$ is given as 1.054 following the formula in Ref. [35]. The efficiency ε_1 (ε_2) is determined to be 1.49% (3.87%) at $\sqrt{s} = 4.23$ GeV and 1.84% (4.37%) at $\sqrt{s} = 4.26$ GeV. Thus, the cross sections are measured to

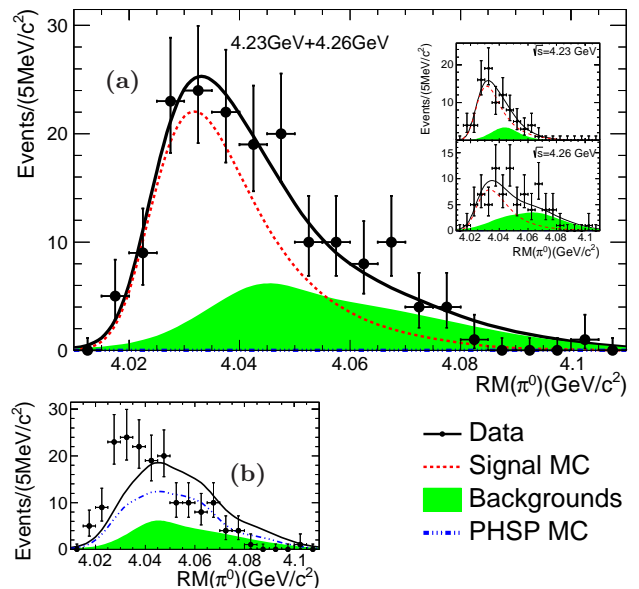


FIG. 2. Fits to $RM(\pi^0)$. (a) A fit to background, PHSP and $Z_c(4025)^0$ signal for the combination of all data (main plot), and the two collision energies separately (inset plots). (b) Fits using only the inclusive background and PHSP. Points with error bars are data, solid line is the sum of fit functions, dotted line stands for the $Z_c(4025)^0$ signals, filled area represents inclusive backgrounds, and dash-dotted line is the PHSP process.

TABLE I. Summary of systematic uncertainties on the $Z_c(4025)^0$ resonance parameters and cross sections σ_{4230} at $\sqrt{s} = 4.23$ GeV and σ_{4260} at 4.26 GeV. “...” means the uncertainty is negligible. The total systematic uncertainty is taken as the root of the quadratic sum of the individual uncertainties.

Source	m (MeV/ c^2)	Γ (MeV)	σ_{4230} (%)	σ_{4260} (%)
Tracking			5	5
Particle ID			5	5
π^0 reconstruction			4	4
Photon veto			4.2	4.2
Mass scale	2.6			
Detector resolution	0.2	0.1	0.3	0.5
Backgrounds	0.6	0.2	5.6	5.4
Oval cut	1.5	1.0	4.2	2.0
Fit range	...	0.1	0.3	0.5
$D^*\bar{D}^*\pi^0$ line shape	6.0	3.0
Luminosity			1	1
\mathcal{B}_1 and \mathcal{B}_2	6.5	5.3
Isospin violation	...	0.2	0.3	0.2
Vacuum polarization			0.5	0.5
Total	3.1	1.0	14.6	12.5

be $(61.6 \pm 8.2) \text{ pb}$ and $(43.4 \pm 8.0) \text{ pb}$ at $\sqrt{s} = 4.23$ and 4.26 GeV, respectively. The contribution of the PHSP process is found to be negligible according to the fit.

Sources of systematic uncertainties in the measurement of the $Z_c(4025)^0$ resonance parameters and cross sections are listed in Table I. Uncertainties of tracking and PID are each 1% per track [36]. The uncertainty

of the π^0 reconstruction efficiency is 4% [37]. We study the photon veto by fitting the recoil mass of $D\pi^0$ with and without this veto in selecting the control sample of $e^+e^- \rightarrow (D^*\bar{D}^*)^0\pi^0$ in data. The efficiency-corrected signal yields are used to extract the cross section, and the corresponding change is taken into account as the systematic error introduced by this requirement. The systematic uncertainties are determined to be 4.2% for both data samples. The mass-scale uncertainty for the $Z_c(4025)^0$ mass is estimated with the mass shift (comparison between the PDG nominal values and fit values) of $RM(D\pi^0)$ in the control sample $e^+e^- \rightarrow D\bar{D}\pi^0$ and of $RM(D)$ in the control sample of $e^+e^- \rightarrow D\bar{D}$. To be conservative, the largest difference of the two mass shifts, $2.6 \text{ MeV}/c^2$, is assigned as the systematic uncertainty due to the mass scale. The systematic uncertainty from backgrounds is estimated by leaving free the magnitudes in the fit and making different choices in non-parametric kernel-estimation of the background events to account for the limited precision in MC simulation [38]. We change the oval cut criteria and take the largest difference as the systematic uncertainty. Since the line shape will affect the efficiency and $(1 + \delta)$, to evaluate the systematic uncertainties with respect to the input $D^*\bar{D}^*\pi^0$ line shape, we change its shape based on uncertainties of the observed $D^{*+}\bar{D}^{*0}\pi^-$ cross section. Branching fractions \mathcal{B}_1 and \mathcal{B}_2 are used in calculating the cross sections and the uncertainties of the world average results are included as part of the systematic uncertainty.

Other items in Table I have only minor effects on the precision of the results. We change the fitting ranges in the $RM(\pi^0)$ spectrum and take the largest difference as the systematic uncertainty. The uncertainties due to detector resolution are accounted for by varying the widths of the smearing functions. The uncertainty of integrated luminosity is determined to be 1% by measuring large angle Bhabha events [7]. We vary the ratio f_k from 0.4 to 0.6 to take into account potential isospin violation between the neutral and charged processes. The corresponding changes are assigned as systematic uncertainties. The systematic uncertainty of the vacuum polarization factor is 0.5% [35].

In summary, using e^+e^- annihilation data at $\sqrt{s} = 4.23$ and 4.26 GeV , we observe enhancements in the π^0 recoil mass spectrum in the process $e^+e^- \rightarrow D^{*0}\bar{D}^{*0}(D^{*+}D^{*-})\pi^0$. Assuming that the enhancement is

due to a neutral charmoniumlike state decaying to $D^*\bar{D}^*$ and it has spin-parity of 1^+ , the mass and width of its pole position are determined to be $m_{\text{pole}}(Z_c(4025)^0) = (4025.5^{+2.0}_{-4.7} \pm 3.1) \text{ MeV}/c^2$ and $\Gamma_{\text{pole}}(Z_c(4025)^0) = (23.0 \pm 6.0 \pm 1.0) \text{ MeV}$, respectively. The Born cross section $\sigma(e^+e^- \rightarrow Z_c(4025)^0\pi^0 \rightarrow (D^{*0}\bar{D}^{*0} + D^{*+}D^{*-})\pi^0)$ is measured to be $(61.6 \pm 8.2 \pm 9.0) \text{ pb}$ at $\sqrt{s} = 4.23 \text{ GeV}$ and $(43.4 \pm 8.0 \pm 5.4) \text{ pb}$ at $\sqrt{s} = 4.26 \text{ GeV}$. Hence, we estimate the ratio $\frac{\sigma(e^+e^- \rightarrow Z_c(4025)^0\pi^0 \rightarrow (D^*\bar{D}^*)^0\pi^0)}{\sigma(e^+e^- \rightarrow Z_c(4025)^+\pi^- \rightarrow (D^*\bar{D}^*)^+\pi^-)}$ to be compatible with unity at $\sqrt{s} = 4.26 \text{ GeV}$, which is expected from isospin symmetry. In addition, the $Z_c(4025)^0$ has mass and width very close to those of the $Z_c(4025)^\pm$, which couples to $(D^*\bar{D}^*)^\pm$ [8]. Therefore, the observed $Z_c(4025)^0$ state in this Letter is a good candidate to be the isospin partner of $Z_c(4025)^\pm$.

The BESIII collaboration thanks the staff of BEPCII and the IHEP computing center for their strong support. This work is supported in part by National Key Basic Research Program of China under Contract No. 2015CB856700; National Natural Science Foundation of China (NSFC) under Contracts Nos. 11125525, 11235011, 11275266, 11322544, 11335008, 11425524; the Chinese Academy of Sciences (CAS) Large-Scale Scientific Facility Program; the CAS Center for Excellence in Particle Physics (CCEPP); the Collaborative Innovation Center for Particles and Interactions (CICPI); Joint Large-Scale Scientific Facility Funds of the NSFC and CAS under Contracts Nos. 11179007, U1232201, U1332201; CAS under Contracts Nos. KJCX2-YW-N29, KJCX2-YW-N45; 100 Talents Program of CAS; INPAC and Shanghai Key Laboratory for Particle Physics and Cosmology; German Research Foundation DFG under Contract No. Collaborative Research Center CRC-1044; Istituto Nazionale di Fisica Nucleare, Italy; Ministry of Development of Turkey under Contract No. DPT2006K-120470; Russian Foundation for Basic Research under Contract No. 14-07-91152; U.S. Department of Energy under Contracts Nos. DE-FG02-04ER41291, DE-FG02-05ER41374, DE-FG02-94ER40823, DESC0010118; U.S. National Science Foundation; University of Groningen (RuG) and the Helmholtzzentrum fuer Schwerionenforschung GmbH (GSI), Darmstadt; WCU Program of National Research Foundation of Korea under Contract No. R32-2008-000-10155-0.

[1] G. T. Bodwin, E. Braaten, E. Eichten, S. L. Olsen, T. K. Pedlar and J. Russ, arXiv:1307.7425; X. Liu, Chin. Sci. Bull. **59**, 3815 (2014); S. L. Olsen, Front. Phys. **10**, 101401 (2015).
[2] S. K. Choi *et al.* [Belle Collaboration], Phys. Rev. Lett. **100**, 142001 (2008).
[3] K. Chilikin *et al.* [Belle Collaboration], Phys. Rev. D **88**, 074026 (2013).

[4] R. Aaij *et al.* [LHCb Collaboration], Phys. Rev. Lett. **112**, 222002 (2014).
[5] M. Ablikim *et al.* [BESIII Collaboration], Phys. Rev. Lett. **112**, 022001 (2014).
[6] M. Ablikim *et al.* [BESIII Collaboration], Phys. Rev. Lett. **110**, 252001 (2013).
[7] M. Ablikim *et al.* [BESIII Collaboration], Phys. Rev. Lett. **111**, 242001 (2013).

- [8] M. Ablikim *et al.* [BESIII Collaboration], Phys. Rev. Lett. **112**, 132001 (2014).
- [9] Z. Q. Liu *et al.* [Belle Collaboration], Phys. Rev. Lett. **110**, 252002 (2013).
- [10] T. Xiao *et al.* Phys. Lett. B **727**, 366 (2013).
- [11] D. Y. Chen, X. Liu and T. Matsuki, Phys. Rev. D **88**, 036008 (2013).
- [12] Z. F. Sun, J. He, X. Liu, Z. G. Luo and S. L. Zhu, Phys. Rev. D **84**, 054002 (2011).
- [13] Z. F. Sun, Z. G. Luo, J. He, X. Liu and S. L. Zhu, Chin. Phys. C **36**, 194 (2012).
- [14] Q. Wang, C. Hanhart and Q. Zhao, Phys. Rev. Lett. **111**, 132003 (2013).
- [15] F. K. Guo, C. Hidalgo-Duque, J. Nieves and M. Pavon Valderrama, Phys. Rev. D **88**, 054007 (2013).
- [16] J. R. Zhang, Phys. Rev. D **87**, 116004 (2013).
- [17] Q. Y. Lin, X. Liu and H. S. Xu, Phys. Rev. D **88**, 114009 (2013).
- [18] X. Wang, Y. Sun, D. Y. Chen, X. Liu and T. Matsuki, Eur. Phys. J. C **74**, 2761 (2014).
- [19] A. Martinez Torres, K. P. Khemchandani, F. S. Navarra, M. Nielsen and E. Oset, Phys. Rev. D **89**, 014025 (2014).
- [20] T. Xiao, S. Dobbs, A. Tomaradze and K. K. Seth, Phys. Lett. B **727**, 366 (2013).
- [21] M. Ablikim *et al.* [BESIII Collaboration], arXiv:1506.06018.
- [22] M. Ablikim *et al.* [BESIII Collaboration], Phys. Rev. Lett. **113**, 212002 (2014).
- [23] M. Ablikim *et al.* [BESIII Collaboration], arXiv:1503.03408.
- [24] M. Ablikim *et al.* [BESIII Collaboration], Nucl. Instrum. Meth. A **614**, 345 (2010).
- [25] C. Zhang, Sci. China. G **53**, 2084 (2010).
- [26] S. Jadach, B. F. L. Ward and Z. Was, Phys. Rev. D **63**, 113009 (2001).
- [27] K. A. Olive *et al.* [Particle Data Group], Chin. Phys. C **38**, 090001 (2014).
- [28] D. J. Lange, Nucl. Instrum. Meth. A **462**, 152 (2001); R. G. Ping, Chin. Phys. C **32**, 599 (2008).
- [29] J. C. Chen, G. S. Huang, X. R. Qi, D. H. Zhang and Y. S. Zhu, Phys. Rev. D **62**, 034003 (2000).
- [30] Charge conjugation is always implied, unless stated specially.
- [31] S. Agostinelli *et al.* [GEANT4 Collaboration], Nucl. Instrum. Meth. A **506**, 250 (2003).
- [32] N. N. Achasov and G. N. Shestakov. Phys. Rev. D **86**, 114013 (2012).
- [33] K. S. Cranmer, Comput. Phys. Commun. **136**, 198 (2001).
- [34] E. A. Jadach and V. S. Fadin, Sov. J. Nucl. Phys. **41**, 466 (1985).
- [35] S. Actis *et al.*, Eur. Phys. J. C **66**, 585(2010).
- [36] M. Ablikim *et al.* [BESIII Collaboration], Phys. Rev. D **83**, 112005 (2011).
- [37] M. Ablikim *et al.* [BESIII Collaboration], Phys. Rev. D **81**, 052005 (2010).
- [38] Kyle S. Cranmer, arXiv:hep-ex/0011057.